PAPER

Check for updates

Controllable synthesis of mesoporous titanosilicates for styrene oxidization using a nanocellulose template strategy†

Dazhi Shen, Jian Liu, [ID]* Lihui Gan, Naizhong Huang and Minnan Long*

In this work, mesoporous titanosilicates with tunable pore size were successfully synthesized using green and cheap bio-templates (nanocellulose). A series of samples was systematically prepared, characterized and used as catalysts for styrene oxidation by H_2O_2. The results demonstrated that the nanocellulose template strategy reported here was a feasible and effective method. The as-prepared titanosilicates presented high specific surface areas (450–500 m^2 g^{-1}) and their mesopore sizes could be tuned from 2 to 8 nm by varying the addition amount of templates in the synthesis process. Active tetrahedral Ti species were efficiently incorporated in the mesoporous silica. Meanwhile, strong acid sites of the samples were confirmed using NH_3-TPD. The catalytic results revealed that the optimal catalysts (Si/Ti = 20 mol ratio) showed high catalytic activity and product selectivity can be adjusted through changing the mesopore size of the catalysts. The recycling tests indicated that as-prepared catalysts exhibited low catalytic deactivation. In addition, the oxidation mechanism over this catalyst was proposed. Thus, the present novel, sustainable and controllable method showed potential practical applications.

1. Introduction

Since the discovery of titanosilicate-1 (Ts-1) in 1983, Ti incorporated zeolitic materials have received much attention due to their remarkable catalytic activity, and created an environmentally friendly route for the oxidation of organic compounds using hydrogen peroxide in mild conditions.[1,2] However, owing to the fact that the pore sizes of conventional microporous titanosilicate zeolites (Ts-1, Ts-2 or other microporous titanosilicates) are smaller than 1 nm,[3] large organic molecules cannot assess the active sites located inside the cavities which limits the utilization of microporous titanosilicates. To overcome this drawback, mesoporous titanosilicates have been developed and proved to be potential catalysts in a wide range of oxidation reactions, especially for bulky organic molecules oxidation. In recently years, many researches have been conducted on synthesis of Ti containing mesoporous silica, such as, Ti-MCM-type,[4–7] Ti-HMS-type,[8–11] Ti-SBA-type,[12–16] *etc.*, and these catalysts have shown excellent catalytic properties in oxidization reaction including hydroxylation of aromatics,[3] oxidative desulfurization,[17] oxidation of alkenes[18] and so on. Nevertheless, these catalysts suffer from cumbersome synthesis procedures and high cost of templates. Especially for latter, the template agents, such as cetyltrimethyl ammonium bromide,

pluronic triblock copolymer and 1-aminododecanelaurylamine, are all from nonrenewable petroleum-based feed stocks and high cost which limited their large-scale application. Therefore, it is still of great significance to develop a simple, green and cost-effective method by using renewable template materials as an environmentally benign alternative. In this respect, biomaterials, in particular cellulose, attracts special attention as a renewable, inexpensive "green" template.[19–21]

Cellulose is one of the most abundant nature material on the earth, which is sustainable, biodegradable and inexpensive sources.[22,23] When cellulose fibers are subjected to acid hydrolysis, stable suspensions of nanocellulose are obtained. Nanocellulose is rod-like or ribbon-like object with a length typically ranging from 50 to 1000 nm and a width varying from 3 to 50 nm.[24–26] Due to possessing nanoscale dimension, high specific strength, high surface area, unique nanosize and accessible industrially in large scale, nanocellulose has been considered as a most promising renewable nanomaterials.[27–29] Recently, nanocellulose has been attracted people's interests in synthesizing mesoporous materials.[30–32] As a kind of nature biological materials, nanocellulose is different from traditional template agents. In addition, it has high aspect ratio, low density and active surface of hydroxyl groups. Thus it possesses the advantages of traditional soft template and hard template at the same time.[33]

In present work, we demonstrate a facile and sustainable method for the synthesis of titanosilicates with tunable mesopore sizes and high specific surface areas by using nanocellulose as the template for the first time. The characterization

College of Energy, Xiamen University, Xiamen, 36105, China. E-mail: jianliu@xmu.edu.cn; longmn@xmu.edu.cn; Fax: +86-592-2188053; Tel: +86-592-5952787

† Electronic supplementary information (ESI) available. See DOI: 10.1039/c7ra01598d

results revealed that active framework Ti species have effectively incorporated in the mesoporous silicate. Further research illustrated that the pore size of as-synthesized mesoporous titanosilicates was controllable. Finally, oxidation of styrene was adopted as a probe reaction to evaluate the catalysts properties of obtained titanosilicates.

2. Experimental

2.1. Chemical and materials

Cellulose from absorbent cotton, sulphuric acid, tetraethylorthosilicate (TEOS), tetrabutyl orthotitanate (TBOT), acetylacetone, styrene, hydrogen peroxide (30% w/v), acetonitrile. All reagents was purchased from Shanghai Chemical Reagent Co. Ltd. (Shanghai, China) and used as received without further purification.

2.2. Synthesis of titanosilicates

Suspensions of nanocellulose (NCC) were prepared as the previous literature,[34] with slight modification. In typical, ten gram of cotton was treated with 100 ml of 65% (w/w) H_2SO_4 at 45 °C for 120 min under vigorous stirring. After that, the obtained nanocellulose suspension was diluted for 5-fold with deionized water to terminate the hydrolysis. The final aqueous suspensions were sonicated for 20 min. The final aqueous suspensions were approximately 1.2% NCC concentration by weight.

One-pot synthesized titanium-silicate with various Ti loading and pore size. In typically, 20 ml of ethanol, 10 ml TEOS, specified mixture of acetylacetone and TBOT (molar ratio of acetylacetone/TBOT = 1/1) were thoroughly mixed at room temperature. The molar composition of the mixture was 1 TEOS: 0.01–0.1 TBOT: 0.01–0.1 acetylacetone: 7.2 ethanol. To this solution, specified volume of as-prepared nanocellulose suspensions (1.2% wt) were added with vigorous stirring. The final solution was further stirred at room temperature for 2 h, and the resulting mixture formed a gel in an oven at 100 °C for 10 h. Finally, the product obtained was washed with deionized water and calcined at 550 °C for 5 h in air to remove the biotemplate incorporated in the composites. After that, the obtained samples were crushed in an agate mortar. As a result, the samples obtained were denoted as Ts-$X(Y)$, where X = 10, 20, 60 or 100 corresponding to the Si/Ti molar ratio and Y = 0.5, 1.5 or 3.0 corresponding to the volume ratio of nanocellulose suspensions to TEOS.

2.3. Characterization

Transmission electron microscopy (TEM) images were obtained on Zeiss Libra200FE operated at 200 kV. XRD spectra of catalysts were acquired on a Rigaku Ultima IV X-ray diffractometer with Ni-filtered Cu Kα radiation operated at 40 kV and 30 mA. The data was collected from 2θ = 10° to 90° at a scan rate of 10° min^{-1}. The nitrogen adsorption and desorption isotherms were measured on an ASAP 2020 system in static measurement mode. The samples were degassed at 300 °C for 4 h before the measurement. The specific surface area of sample was

calculated by BET model. The pore size distribution curves were obtained by the BJH (Barrett–Joyner–Halenda) method based on the adsorption branch of isotherm. The diffuse reflectance UV-vis spectra were recorded on a VARIAN Cary 5000 spectrometer equipped with a diffuse reflectance attachment and using $BaSO_4$ as a reference. FT-IR spectra were recorded on a Nicolet iS5 spectrometer. NH_3-TPD was measured by using a Micromeritics AutoChem II 2920 equipped with a thermal conductivity detector (TCD).

2.4. Catalytic activity

The catalytic tests were performed in a sealed round bottom flask in which vigorous stirring at 80 °C. Typically, the reactor was charged with 200 μl styrene, 2 ml of acetonitrile as solvent, specified hydrogen peroxide and 0.08 g catalyst loading. The oxidation products were analyzed by gas chromatography on Agilent 7890. After the reactions, the catalyst was separated by centrifugation, washed with acetonitrile for three times and dried at 100 °C for 6 h to be reused.

3. Results and discussion

3.1. Catalyst characteristics

Fig. 1 shows the XRD spectra of the samples with different Si/Ti molar ratio. As seen, all the curves show a relatively weak diffraction band at the 2θ range of 15–35°, which is associated with the amorphous silica materials.[15,35] Additional peaks characteristic of TiO_2 are not detected in all samples. The result indicates that the separate TiO_2 phase is absent in the samples.

UV-vis diffuse reflectance spectroscopy has been used to study the environment of titanium in amorphous silica in the wavelength range of 200 nm to 800 nm. As seen in Fig. 2, the maxima of absorption band of all samples center at 220 nm together with a weak shoulder band at 270 nm. The band at 220 nm can be attributed to tetrahedral Ti species and the shoulder band at 270 nm indicate the presence of titanium in an octahedral coordination environment.[6] Absorbance value of two bands suggests that a major of titanium species presents in tetrahedral and accompanies by a less fraction in octahedral coordination.[3] Moreover, the absorption bands are not detected in the range of 350–400 nm indicating that the presence of a free TiO_2 clusters or extra-framework anatase TiO_2 species in all
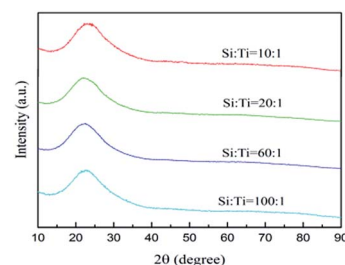

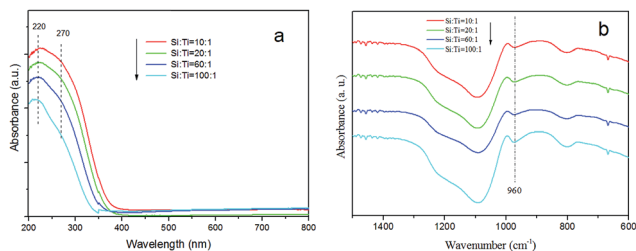Fig. 1 XRD patterns of titanosilicates synthesized with different Si/Ti molar ratio.

Fig. 2 (a) UV-vis spectra and (b) FT-IR spectra of titanosilicates with different Si/Ti mole ratios.

samples can be ruled out,[17] which are in good agreement with the XRD results.

The FT-IR spectra of the samples are shown in Fig. 2b. All samples appear a band at 960 cm^{-1} which can be associated with the framework Si–O–Ti vibrations.[2] The existence of Si–O–Ti indicates that the Ti species are incorporation into the framework which would supply active sites on catalyst. The result further confirms that active framework Ti species have efficiently incorporated in the mesoporous silica.

In this work, the samples have been synthesized under acidic precursor solution conditions which is from the acidic nano-cellulose suspension solution. The pH of the synthesis precursor solutions are in the range of 0.2–0.4. The silica/Ti precursor will hydrolysis under the action of acid catalyst.[36] However, it is well known that the hydrolysis of silica precursor (TEOS) is slower than that of titanium precursor (TBOT). To avoid the incongruous hydrolysis rates, acetylacetone has been used as a chelating agent to ensure active framework Ti species efficiently incorporating into the framework of silica rather than separate TiO$_2$ crystals.

Fig. 3a and b show the N$_2$ adsorption–desorption isotherms and the pore size distribution for the samples with different Si/
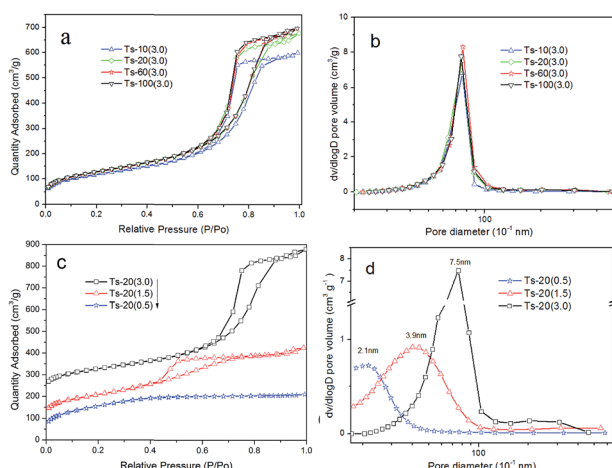
Ti ratios. As can be seen, all products show type-IV curves[37] with a narrow distribution of mesoporous diameters centering at about 7.5 nm. Specific surface areas and pore volume change slight at Si/Ti = 100, 60 and 20 while they decrease prominently at Si/Ti = 10. These changes could be observed clearly in Table 1 (entry 1–4). This result indicates that titanium incorporated in SiO$_2$ framework has little effect on the mesoporous structure at high Si/Ti ratio. However, excessive-loading of titanium (Si/Ti = 10) in the sample could also induce a reduction in BET surface area and pore volume.

The influence of templates ratio on the morphology and pore structure has been investigated. The results are showed in Fig. 3c and d, and the corresponding parameters are listed in Table 1 (entry 5–7). The pore diameter and pore volume significantly increase with the addition amount of nano-cellulose templates in precursor solution. Subsequently, the specific surface areas of the samples slightly decrease. These results confirm that the pore size of the catalysts can be systematically adjusted by varying the amounts of bio-template (nanocellulose) in the synthesis system.

Fig. 4 gives the TEM images of as-prepared samples with the NCC/TEOS ratio at 0.5, 1.5 and 3, respectively. The synthesized samples show the patterns characteristic of disorder wormhole-like meso-structure. The similar structure was also observed by previously reports.[38,39]

The property of acid sites is determined by NH$_3$-TPD (Fig. 5). Two major desorption peaks are observed at 150–250 °C and 300–800 °C in Fig. 5. The former can be attributed to ammonia desorbed from weaker acid centers, and the latter was from relatively stronger acid centers. The acidic sites of the samples can be attributed the unsaturated Ti^{4+} species at surface defect sites of the catalysts.[15,40]

3.2. Catalytic performances of catalysts

3.2.1 Effect of Si/Ti ratio. Finally, the catalytic performance of as-synthesized samples are evaluated through oxidation of styrene by using 30 wt% H$_2$O$_2$ as an oxidant. The main products of the reaction are benzaldehyde, 1-phenyl-1,2-ethanediol and benzoic acid. The effect of catalysts in different Si/Ti mole ratio catalysts is investigated and the results are presented in Fig. 6a. Obviously, the catalytic activity (styrene conversion) increases firstly with the increasing of Ti content but then drop. The optimum result is at Si/Ti = 20 with the highest conversion of 71.3%. It is reasonable that the activity site increase with the Ti content. However, the catalytic activity does not increase at Si/Ti = 10. The result may be mainly due to the decreased specific surface areas of the sample (Table 1, entry 1), which reduce the activity sites on the surface of the catalysts.

3.2.2 Effect of pore size. Catalysts with three different pore sizes at the Si/Ti = 20 were evaluated and the results are shown in Fig. 6b. The catalysts Ts-20(0.5) and Ts-20(1.5) exhibit almost the same conversions (73.5% and 74.4%, respectively) which can be attributed to their similar specific surface areas. Owing to the relative low specific surface areas of Ts-20(3.0) compared with the Ts-20(0.5) and Ts-20(1.5), the conversion correspondingly decrease to 71.3%. As for the effects of pore size on

Fig. 3 N$_2$ adsorption and desorption isotherms of mesoporous titanosilicates with different Si/Ti ratio (a), corresponding pore size distribution (b), different CNC/TEOS ratio (c) and corresponding pore size distribution (d). The isotherms for products Ts-20(1.5) and Ts-20(30) were vertically offset by 70 and 200 cm^3 g^{-1}, respectively in part (c).

Table 1 Textural characterization of as-prepared titanosilicates

Entry	Cat.	Si/Ti (mole ratio)	NCC/TEOS (v/v)	S ($m^2\ g^{-1}$)	DBJH[a] (nm)	V_p[b] ($cm^3\ g^{-1}$)
1	Ts-10(3.0)	10	3	425.1	7.6	0.93
2	Ts-20(3.0)	20	3	463.9	7.5	1.05
3	Ts-60(3.0)	60	3	462.6	7.5	1.09
4	Ts-100(3.0)	100	3	466.2	7.4	1.08
5	Ts-20(0.5)	20	0.5	516.9	2.1	0.32
6	Ts-20(1.5)	20	1.5	500.5	3.9	0.55
7	Ts-20(3.0)	20	3	463.9	7.5	1.05

[a] Pore diameter (obtained from the adsorption isotherm by the BJH method). [b] Pore volume determined by nitrogen adsorption at a relative pressure of 0.98.
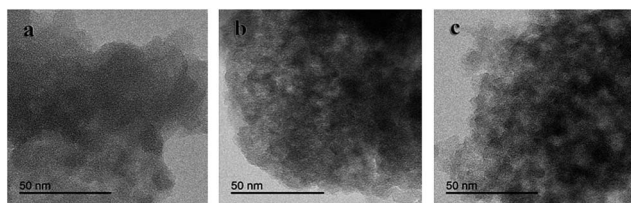

Fig. 4 TEM images of the samples. Ts-20(0.5) (a), Ts-20(1.5) (b) and Ts-20(3.0) (c).

products distribution, the Ts-20(3.0) with the pore size at 7.5 nm gave a better performance in selectivity for benzaldehyde than other catalysts. Whereas, the Ts-20(0.5) with the pore size at 2.1 nm show a better selectivity for 1-phenyl-1,2-ethanediol. This result indicates that different pore size of the catalysts has an obvious effect on the reaction. Thus, as-prepared catalysts with tunable pore size will be advantageous to adjust the selectivity of the products.

3.2.3 Effect of H_2O_2/styrene. The sample Ts-20(3.0) was chosen to investigate the influences of H_2O_2/styrene mole ratio and the results are shown in Fig. 6c. It is obvious that an increased oxidant/reactant ratio leads to the facilitation of styrene conversion. With the H_2O_2/styrene ratio increasing from 1.5 to 3, the conversion of styrene increase from 63.5% to 86.3%. But simultaneously, the selectivity for 1-phenyl-1,2-ethanediol decrease obviously from 24.9% to 15.3% and, benzaldehyde and benzoic acid selectivity rise.

3.2.4 Effect of reaction time. Fig. 6d showed the effect of reaction time on styrene oxidation using Ts-20(3.0). It was found that styrene conversion increased rapidly from 46.3 to
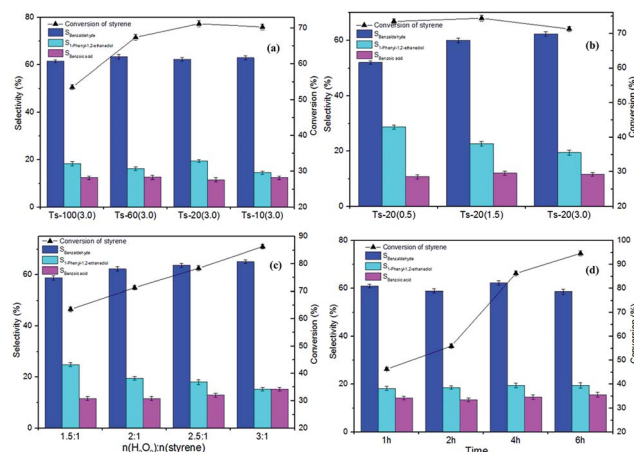

Fig. 5 NH$_3$-TPD spectra of Ts-20(0.5); Ts-20(1.5); Ts-20(3.0).

Fig. 6 Catalytic performances on the oxidization of styrene. (a) Effect of Ti/Si ratio (80 °C, 4 h, H_2O_2/styrene = 2); (b) effect of pore size of catalysts (80 °C, 4 h, H_2O_2/styrene = 2); (c) effect of the H_2O_2/styrene (catalyst: Ts-20(3.0), 80 °C, 4 h); (d) effect of reaction time (catalyst: Ts-20(3.0), 80 °C, H_2O_2/styrene = 3).

86.3% with prolongation of reaction time from 1 to 4 h. Only little increment was observed when reaction time was prolonged to 6 h. Moreover, the product distribution showed little changes with reaction time.

3.2.5 Proposed mechanism of oxidation reaction. It is well accepted that the oxidation of styrene at the side chain can obtain different products depending on the catalysts and reaction conditions. According to previous reports,[41–43] we proposed that the reaction process may have two major reaction routes (Scheme 1). On the presence of catalysts, benzaldehyde, 1-phenyl-1,2-ethanediol and benzoic acid are detected in the oxidation products. The main product is benzaldehyde, which is from the direct oxidative cleavage of the styrene side chain double bond[40] (route 1, Scheme 1). Benzaldehyde can also be from a oxidization of epoxystyrene (route 2–1, Scheme 1), and it is also readily oxidized to benzoic acid.[41] It is interesting that epoxystyrene is not detected in products compared with previous reports.[2,18] This can be ascribed to the existence of acid site on our catalysts and the subsequent hydrolysis of epoxy group.[44] Therefore, the product of 1-phenyl-1,2-ethanediol is derived from the hydrolysis of the epoxystyrene (route 2–2, Scheme 1). Furthermore, there is a competition between the
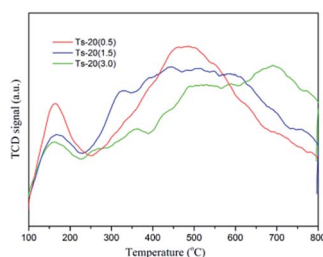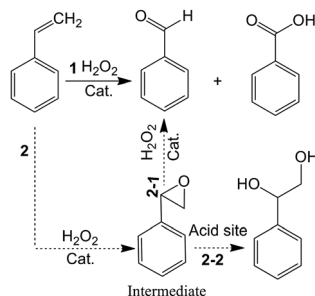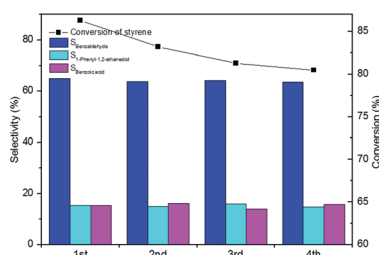
Scheme 1 Proposed reaction mechanism of styrene oxidation.

Fig. 7 Catalyst reusability (Ts-20(3.0); H_2O_2/styrene = 3; 80 °C; 4 h.)

oxidation (route 2–1) and hydrolysis of epoxystyrene (route 2–2, Scheme 1), which is in good agreement with our experimental results that if more oxidant (H_2O_2) is employed in the reaction, the selectivity of benzaldehyde increases, while the selectivity of 1-phenyl-1,2-ethanediol decreases.

It is noted that pore sizes of the catalysts have a prominent effect on product selectivity in this work. This phenomenon can be attributed to the effect of diffusion of the reaction species in different catalysts pore size. The catalysts (Ts-20(3.0)) with macropores tend to oxidization reaction for the fast diffusion of reactants in the pores. Thus, the catalysts (Ts-20(3.0)) have higher selectivity for oxidation product than the others. In contrast, narrow pore channel on the catalysts (Ts-20(0.5)) inhibits further oxidization of the intermediate (epoxystyrene) owing to the poor diffusion which will cause more hydrolysis of intermediate (epoxystyrene, route 2–2, Scheme 1) on the acid site of the catalysts. Thus, the catalyst (Ts-20(0.5)) has the best selectivity for hydrolysis product (1-phenyl-1,2-ethanediol).

3.2.6 Catalyst reusability. In order to characterize the durability of the catalysts, the recycling of the catalyst was carried out. The catalysts (Ts-20(3.0)) was chosen and evaluated in four recycling experiments. As seen from Fig. 7, the catalyst is quite stable even in the 4th recycle. The conversion is still remained 80% and little variation in products selectivity is detected. Furthermore, we find that this catalyst (Ts-20(3.0)) gave competitive activity compared with previous reports (see the ESI, Table S1†).

4. Conclusions

In this article, we demonstrated a novel, facile and controllable method for synthesis of mesoporous titanosilicates by using bio-template (nanocellulose) for the first time. As-prepared titanosilicates are proved with high surface areas (450–500 m^2 g^{-1}) and tunable pore size (2–8 nm). Active framework Ti has effectively incorporated in the frameworks of silicate. Meanwhile, strong acid sites of the samples have been confirmed by NH_3-TPD. The catalyst tests illustrate that the optimum Si/Ti atom ratio is 20 and product selectivity can be adjusted through changing the mesopore size of the catalysts. The recycling tests indicate that the catalysts exhibit low catalytic deactivation. Hence, the catalysts synthesized with presenting method will be advantageous to general applications in various molecular catalysis due to their tunable pore size.

Acknowledgements

References

1 F. Jin, S. Y. Chen, L. Y. Jang, J. F. Lee and S. F. Cheng, *J. Catal.*, 2014, **319**, 247–257.

2 J. J. Wang, J. M. Lu, J. H. Yang, R. Chen, Y. Zhang, D. H. Yin and J. Q. Wang, *Appl. Surf. Sci.*, 2013, **283**, 794–801.

3 A. Kumar and D. Srinivas, *J. Mol. Catal. A: Chem.*, 2013, **368**, 112–118.

4 R. Peng, D. Zhao, N. M. Dimitrijevic, T. Rajh and R. T. Koodali, *J. Phys. Chem. C*, 2012, **116**, 1605–1613.

5 J. Silvestre-Albero, M. E. Domine, J. L. Jorda, M. T. Navarro, F. Rey, F. Rodriguez-Reinoso and A. Corma, *Appl. Catal., A*, 2015, **507**, 14–25.

6 J. M. Fraile, N. García, J. A. Mayoral, F. G. Santomauro and M. Guidotti, *ACS Catal.*, 2015, **5**, 3552–3561.

7 K. F. Lin, P. P. Pescarmona, H. Vandepitte, D. Liang, G. Van Tendeloo and P. A. Jacobs, *J. Catal.*, 2008, **254**, 64–70.

8 Y. Wang, G. Li, X. S. Wang and C. Z. Jin, *Energy Fuels*, 2007, **21**, 1415–1419.

9 B. Pawelec, J. L. G. Fierro, A. Montesinos and T. A. Zepeda, *Appl. Catal., B*, 2008, **80**, 1–14.

10 T. A. Zepeda, A. Infantes-Molina, J. N. D. de Leon, R. Obeso-Estrella, S. Fuentes, G. Alonso-Nunez and B. Pawelec, *J. Mol. Catal. A: Chem.*, 2015, **397**, 26–35.

11 Y. B. Zhuang, H. Y. Song, G. Li and Y. J. Xu, *Mater. Lett.*, 2010, **64**, 2491–2493.

12 S. D. Shen, Y. Deng, G. B. Zhu, D. S. Mao, Y. H. Wang, G. S. Wu, J. Li, X. Z. Liu, G. Z. Lu and D. Y. Zhao, *J. Mater. Sci.*, 2007, **42**, 7057–7061.

13 F. Berube, B. Nohair, F. Kleitz and S. Kaliaguine, *Chem. Mater.*, 2010, **22**, 1988–2000.

14 R. V. Sharma, K. K. Soni and A. K. Dalai, *Catal. Commun.*, 2012, **29**, 87–91.

15 A. Kumar and D. Srinivas, *J. Catal.*, 2012, **293**, 126–140.

16 S.-Y. Chen, T. Mochizuki, Y. Abe, M. Toba and Y. Yoshimura, *Applied Catalysis B: Environmental*, 2014, **148–149**, 344–356.

17 T. W. Kim, M. J. Kim, F. Kleitz, M. M. Nair, R. Guillet-Nicolas, K. E. Jeong, H. J. Chae, C. U. Kim and S. Y. Jeong, *Chemcatchem*, 2012, **4**, 687–697.

18 M. Fadhli, I. Khedher and J. M. Fraile, *J. Mol. Catal. A: Chem.*, 2016, **420**, 282–289.

19 S. J. Eichhorn, A. Dufresne, M. Aranguren, N. E. Marcovich, J. R. Capadona, S. J. Rowan, C. Weder, W. Thielemans, M. Roman, S. Renneckar, W. Gindl, S. Veigel, J. Keckes, H. Yano, K. Abe, M. Nogi, A. N. Nakagaito, A. Mangalam, J. Simonsen, A. S. Benight, A. Bismarck, L. A. Berglund and T. Peijs, *J. Mater. Sci.*, 2010, **45**, 1–33.

20 P. Tingaut, T. Zimmermann and G. Sebe, *J. Mater. Chem.*, 2012, **22**, 20105–20111.

21 D. Klemm, F. Kramer, S. Moritz, T. Lindstrom, M. Ankerfors, D. Gray and A. Dorris, *Angew. Chem.*, 2011, **50**, 5438–5466.

22 Y. Hu, L. Tang, Q. Lu, S. Wang, X. Chen and B. Huang, *Cellulose*, 2014, **21**, 1611–1618.

23 H.-M. Ng, L. T. Sin, T.-T. Tee, S.-T. Bee, D. Hui, C.-Y. Low and A. R. Rahmat, unpublished work.

24 M. Kaushik and A. Moores, *Green Chem.*, 2016, **18**, 622–637.

25 Q. Q. Li, S. McGinnis, C. Sydnor, A. Wong and S. Renneckar, *ACS Sustainable Chem. Eng.*, 2013, **1**, 919–928.

26 M. C. Li, Q. L. Wu, K. L. Song, S. Lee, Y. Qing and Y. Q. Wu, *ACS Sustainable Chem. Eng.*, 2015, **3**, 821–832.

27 K. Oksman, Y. Aitomäki, A. P. Mathew, G. Siqueira, Q. Zhou, S. Butylina, S. Tanpichai, X. J. Zhou and S. Hooshmand, *Composites, Part A*, 2016, **83**, 2–18.

28 N. Lavoine, I. Desloges, A. Dufresne and J. Bras, *Carbohydr. Polym.*, 2012, **90**, 735–764.

29 H. Y. Yu, Z. Y. Qin, C. F. Yan and J. M. Yao, *ACS Sustainable Chem. Eng.*, 2014, **2**, 875–886.

30 B. Paredes, A. Widera, V. Murg, O. Mandel, S. Folling, I. Cirac, G. V. Shlyapnikov, T. W. Hansch and I. Bloch, *Nature*, 2004, **429**, 277–281.

31 E. Dujardin, M. Blaseby and S. Mann, *J. Mater. Chem.*, 2003, **13**, 696–699.

32 K. E. Shopsowitz, H. Qi, W. Y. Hamad and M. J. Maclachlan, *Nature*, 2010, **468**, 422–425.

33 F. Shi, T. Yu, S.-C. Hu, J.-X. Liu, L. Yu and S.-H. Liu, *Chem. Eng. J.*, 2016, **292**, 105–112.

34 S. Beck-Candanedo, M. Roman and D. G. Gray, *Biomacromolecules*, 2005, **6**, 1048–1054.

35 S. Y. Chen, T. Mochizuki, Y. Abe, M. Toba and Y. Yoshimura, *Appl. Catal., B*, 2014, **148**, 344–356.

36 M. A. Betiha, H. M. A. Hassan, A. M. Al-Sabagh, A. S. Khder and E. A. Ahmed, *J. Mater. Chem.*, 2012, **22**, 17551–17559.

37 H. L. Chen, Y. P. Peng, K. F. Chen, C. H. Lai and Y. C. Lin, *J. Environ. Sci.*, 2016, **44**, 76–87.

38 T. Witoon, M. Chareonpanich and J. Limtrakul, *Mater. Lett.*, 2008, **62**, 1476–1479.

39 M. A. Betiha, S. A. Mahmoud, M. F. Menoufy and A. M. Al-Sabagh, *Appl. Catal., B*, 2011, **107**, 316–326.

40 S.-Y. Chen, T. Mochizuki, Y. Abe, M. Toba and Y. Yoshimura, *Appl. Catal., B*, 2014, **148–149**, 344–356.

41 V. Hulea and E. Dumitriu, *Appl. Catal., A*, 2004, **277**, 99–106.

42 A. D. S. Neto, L. G. Pinheiro, J. M. Filho and A. C. Oliveira, *Fuel*, 2015, **150**, 305–317.

43 X. C. Zhu, R. W. Shen and L. X. Zhang, *Chin. J. Catal.*, 2014, **35**, 1716–1726.

44 N. T. Thao and L. T. K. Huyen, *Chem. Eng. J.*, 2015, **279**, 840–850.